Optics Letters

Chip-scale humidity sensor based on a silicon nanobeam cavity

Minmin You,[1,2] Zude Lin,[1,2] Fangfang Wang,[1,2] Yiwei Bai,[1,2] Xiuyan Li,[1] Yikai Su,[1] and Jingquan Liu[1,*]

[1]National Key Laboratory of Science and Technology on Micro/Nano Fabrication, Shanghai Jiao Tong University, Shanghai 200240, China
[2]Department of Micro/Nano Electronics, Shanghai Jiao Tong University, Shanghai 200240, China
*Corresponding author: jqliu@sjtu.edu.cn

Received 15 August 2019; revised 21 September 2019; accepted 25 September 2019; posted 2 October 2019 (Doc. ID 375381); published 29 October 2019

In this Letter, a novel humidity sensor based on a chip-scale silicon nanobeam cavity with polymethyl methacrylate (PMMA) cladding is demonstrated. This sensor is easy to fabricate and compatible with CMOS technology. It shows a humidity sensing with a linear wavelength dependence of 22.9 pm/% relative humidity (RH) in a wide range of RH from 10% to 85%, an ultra-fast response time of 540 ms, and high stability. After annealing, the sensor exhibits high reversibility, repeatability, and temperature insensitivity at the range of 25°C–40°C. To the best of our knowledge, this is the first application of integrated photonics in high performance humidity detection. It provides a new way for the chip-scale sensor to integrate with photonic devices and optical systems.

https://doi.org/10.1364/OL.44.005322

Humidity sensing plays a significant role in various fields, such as chemical and biomedical industries, environment monitoring, aerospace, and agriculture [1,2]. Recently, compared with traditional electrical counterparts, humidity sensors based on optical detecting methods have attracted much attention due to the advantages of electromagnetic interference immunity and robustness against mechanical shock. The humidity detection has been achieved by various kinds of optical fibers, such as fiber Bragg grating (FBG) [3], tapered optical fiber (TOF) [4], long period grating (LPG) [5], photonic crystal fiber (PCF) [6], and side polished fiber (SPF) [7]. It has also been suggested that the humidity sensitivity can be improved greatly by replacing traditional polymer with some new sensitive materials [8,9]. However, in the age of optical and electronic devices integration, currently available fiber optical sensors cannot meet the requirements of integration due to being incompatible with CMOS technologies and fragility [10]. In addition, these sensors tend to suffer from strain fluctuation, decreasing the sensing reliability [11]. Moreover, constrained by low quality factors, it is hard to achieve a high resolution of sensing for fiber optical sensors [12]. All of these issues place an obstacle before achieving integrated sensing and precise humidity detecting.

Nowadays, to realize integrated sensing, chip-scale silicon photonics have been widely used in biotechnology, gas, and temperature sensing, such as Bragg gratings, micro-ring resonators, and photonic crystal (PhC) nanobeam cavities [13–15]. Meanwhile, the silicon resonators, with ultra-high quality factors, have an ability to break the resolution limit of sensing in some cases. Some works have shown that a silicon ring resonator can resolve temperature differences of 1 mK based on the temperature-induced refractive index change of silicon [16]. However, since silicon is insensitive to humidity, applying silicon photonics to humidity detection is still challenging. Moreover, the temperature sensitivity of silicon will also seriously influence the accuracy of humidity monitoring. Therefore, silicon photonics-based humidity sensors have not been achieved up to date.

In this work, a humidity sensor based on a silicon PhC nanobeam cavity was designed and investigated. The structure with a modulated stack width can strongly localize the light field in its upper cladding, which substantially improves its sensitivity to the change in cladding refractive index (RI) caused by water absorption. Therefore, polymethyl methacrylate (PMMA), with low optical transmission loss and good hydrophilic properties, was chosen as its upper cladding. The results show that the silicon nanobeam with PMMA cladding can sense humidity with a high sensitivity and an excellent linearity against a wide range of relative humidity (RH). The high sensitivity is achieved by fully taking advantage of electronic field distribution and the hydrophilic property of PMMA. The developed humidity sensor based on a chip-scale silicon nanobeam cavity provides advantages of compactness, a CMOS compatibility, planar structures, and design flexibility. To the best of our knowledge, this work successfully applies silicon resonators to humidity sensing for the first time, which paves a way for the integrated photonics and optical systems in the future.

Figure 1(a) shows the structure of the proposed stack width modulated nanobeam cavity. The design of the cavity followed a deterministic approach referred in Ref. [17]. It consists of rectangle silicon stacks with a lattice constant of 400 nm. The ridge width of the waveguide is 820 nm. The width of the slits and the silicon stacks were designed to be 198 and 202 nm, respectively. The lengths of the rectangles were increased

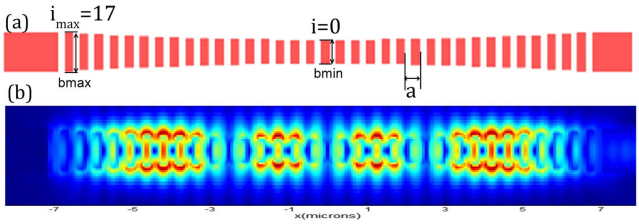

Fig. 1. (a) Top view of the nanobeam cavity. (b) Electric field distribution.

from 500 to 820 nm from the middle of the nanobeam cavity to its two terminals following the formula: $(b(i) + i^2(b_{max} - b_{min})/i^2_{max}$. The number of the stacks i is 17. The electric field distribution of the nanobeam with PMMA cladding was simulated by the three-dimensional finite-difference time-domine (3D-FDTD), as shown in Fig. 1(b). Apparently, this nanobeam cavity strongly localizes its electric field inside its upper cladding, which enhances the interaction between light and PMMA cladding. Thus, the dependence of resonant wavelength on humidity will be intensified. Figure 2(a) schematically shows the fabrication process of the sensor. The device was fabricated using standard CMOS technology on a silicon on insulator (SOI) wafer with a 220 nm silicon core layer on a 2 μm buried SiO2 layer. The grating couplers and the nanobeam cavity were shallowly and fully etched, respectively, by combining electron-beam lithography (EBL, Visten EBPG 5200+) and inductively coupled plasma (ICP) etching (SPTS DRIE-I). Then, the PMMA (AZ 495) was spun with three kinds of thickness, 250 nm, 500 nm, and 1 μm, as its upper cladding. Figures 2(b) and 2(c) show the microscope image and SEM picture of the fabricated sensor.

The experimental setup of humidity sensing is shown in Fig. 3(a). The sensor was enclosed in a plastic chamber in which the humidity was controllable. The chamber was equipped with four holes to get a gas/optics inlet and outlet, respectively. Humid and dry N2 were controlled by two mass controllers, respectively, and flowed into the chamber through the gas inlet. Thus, the RH in the chamber could be adjusted from 0%RH to 100%RH. A commercially purchased humidity sensor (HW-100), with measurement limits of 0%–90% RH,

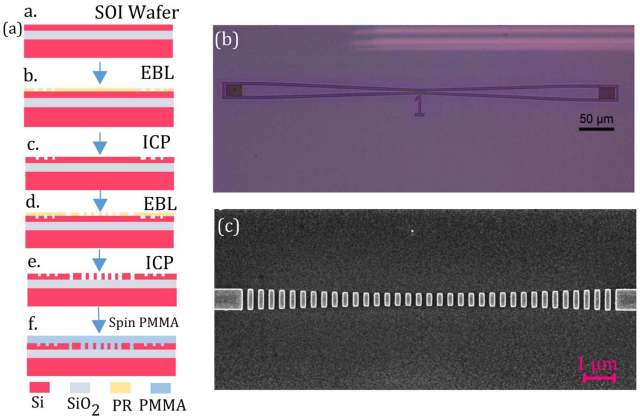

Fig. 2. (a) Fabrication process. (b) Optical microscope image of the fabricated humidity sensor. (c) SEM photos of the nanobeam cavity.

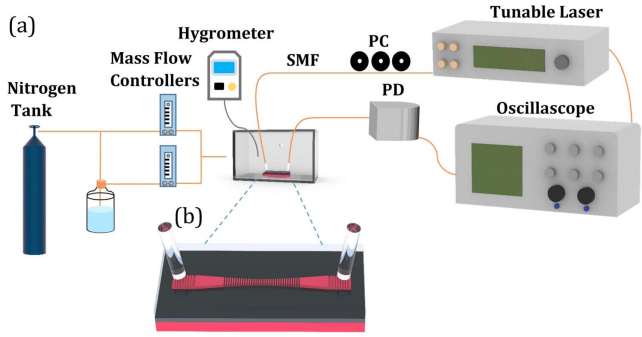

Fig. 3. (a) Schematic diagram of experimental setup. (b) Magnified 3D view of the fabricated humidity sensor.

monitored the humidity in the chamber in real time. Through the optics holes, the optical fibers could couple the light in and out from the silicon chip by means of the 4 dB grating couplers. The tunable laser (NEW PORT TLB-6728) was used to pump the nanobeam cavity, and the output light was immediately detected by a photo detector (NEW PORT 0901). Meanwhile, the oscilloscope (KESIGHT) was used to collect the input and output signal. To eliminate the influence of temperature fluctuations, all experiments were carried out at room temperature (25 ± 0.8°C).

To analyze the influence of cladding thickness, the nanobeam cavity with a different thickness of PMMA (250 nm, 500 nm and 1 μm) was studied. Figure 4(a) shows their normalized transmission spectrum at 32.1% RH. It performs an obvious red shift on resonant wavelength for the sensors with thicker PMMA cladding. The shift is caused by the change of the effective refractive index (n_{eff}) as follows:

$$\lambda_{res} = 2n_{eff} \cdot a, \tag{1}$$

where λ_{res} represents resonant wavelength, a is lattice constant, and n_{eff} is the effective refractive index. It illustrates that the n_{eff} grows up with the increase of the thickness of PMMA, which induces a great red shift in resonant wavelength. The experimental results agree with the theory. Two resonant peaks could be identified clearly as the longitudinal mode with the first and second, respectively. A magnified view of the first resonant peak with 500-nm-thick PMMA is illustrated in Fig. 4(b). It has a full width at half maximum (FWHM) of 330 pm, indicating a Q factor of 4660. The performance is greatly improved compared with traditional optical fiber sensors with a low quality factor of 700 [9], which is a promotion for realizing high

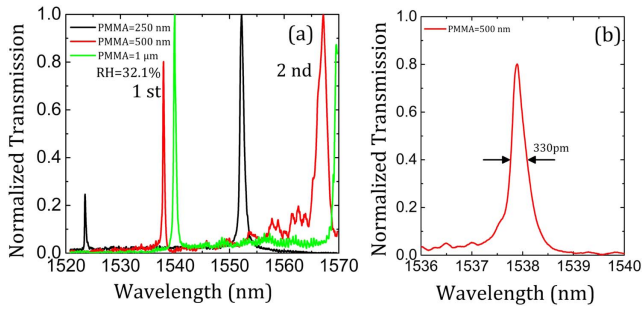

Fig. 4. (a) Normalized spectrum transmission of the fabricated humidity sensors. (b) Magnified view of the resonant peak.

resolution of humidity measurements. Considering that the Q factor is relatively high at 1537.890 nm, the following analysis is carried out around this resonant peak.

Figure 5(a) shows the transmission spectrum of the fabricated humidity sensor with 500-nm-thick PMMA at different RH. With the increase of the relative humidity, the resonant wavelength has an obvious red shift of 2 nm. This is because once the water molecules were absorbed into the hydrophilic PMMA, the refractive index factor of the upper cladding raised up, causing a red shift in resonant wavelength as expected from Eq. (1). The fluctuations in FWMH for the different RH also resulted from it, while it has no effect on sensitivity in our measurement by analysis. The relationship between the resonant wavelength of nanobeam cavities (PMMA = 250 nm, 500 nm, 1 μm) and relative humidity is shown in Fig. 5(b). The resolution and uncertainty of our experimental setup for the transmission spectrum is 5 pm and 10 pm, respectively. For the sensor with 500-nm-thick PMMA, the resonant wavelength performs a high humidity sensitivity of 22.94 ± 1.99 pm/%RH with relative humidity in the whole range. The calculated resolution of humidity detection is 0.217% RH and the uncertainty is 3.1%RH. Benefiting from the introduction of the special stack width modulated nanobeam cavity, the proposed sensor exhibits an obvious improvement on humidity sensitivity compared with reported fiber optical sensors with PMMA cladding. Figure 5(b) also shows the dependence of resonant wavelength on relative humidity with different thicknesses of PMMA. The linear sensitivities of 18.82 ± 1.75 pm/%RH and 17.69 ± 1.64 pm/%RH are obtained for 250-nm-thick and 1-μm-thick PMMA, respectively. The experimental results indicate that the thickness of PMMA cladding has a weak influence on the humidity sensitivity. The deep explanation of this phenomenon should be further studied. In the following analysis, we focus on the humidity sensor with 500-nm-thick PMMA.

The response time and stability of the humidity sensor were investigated considering that the shift of resonant wavelength can be translated into the intensity change of output light with a fixed light source when RH is changed. The output wavelength was fixed at a resonant peak of 1538.998 nm. The output light was detected in real time by a photo detector, and the humidity was changed from 75% RH ($\lambda_{res} = 1538.897$ nm) to 60.8%RH. The response of output light to humidity is synchronously recorded by oscilloscope, as shown in Fig. 6(a). A clear decreasing and increasing of the light intensity were observed in real-time with the falling and rising of humidity in the range of 75%RH–60.8%RH, respectively. That is because the drop of humidity induces a blue shift in resonant

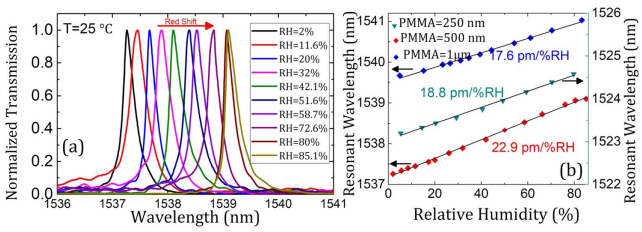

Fig. 5. (a) Measured normalized spectrum transmission at different relative humidity. (b) Linear fitting of experimental data versus relative humidity with different thickness of PMMA cladding.

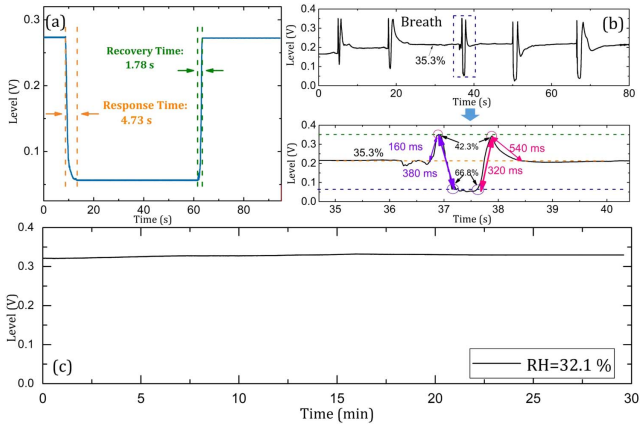

Fig. 6. (a) Response and recovery time of the humidity sensor. (b) Fast response to human breath. (c) Output voltage fluctuation over a period of time at room humidity.

wavelength, and the voltage of output light decreases accordingly. This sensor exhibits a response time of 4.73 s and a recovery time of 1.78 s. Considering that the response time could be constrained by our experimental setup, Fig. 6(b) further presents its fast response to human breath. By fixing the output wavelength at 1538.129 nm, the detected output signal correspondingly changes with five repetitive cycles of respiratory responses over a period of 60 s. Two sharp peaks emerged in each cycle are attributed to exhaling and inhaling respectively. When breaths are on, a red shift of the resonant wavelength ($\lambda_{res} = 1537.890$ nm) is induced. Thus, the output voltage first increases with the red shift, followed by a rapid decrease once the resonant wavelength exceeds the fixed wavelength (1538.129 nm). As for breathing off, the process is the opposite. Purple and rose are used to label these two processes, respectively, as shown in the enlarged view in Fig. 6(b). According to the transmission spectrum of the resonant peak, the output voltage variation can be translated into the shift in resonant wavelength. Then the value of humidity at a critical point can be calculated by combing the relationship between relative humidity and resonant wavelength. Four points of inflexion correspond to 42.3%RH and 66.8%RH, respectively. An extremely sharp rise (160 ms) and relatively quick drop (380 ms) show its rapid response to human breath. In the relative humidity range of 35.3%RH–66.8%RH, the fabricated sensor exhibits an ultra-fast response time of 540 ms and recovery time of 860 ms. It performs an outstanding advantage compared with the reported humidity sensor [18,19]. In order to study the stability of the humidity sensor, we recorded the variation of the output voltage versus time at room humidity, as illustrated in Fig. 6(c). The input wavelength was tuned to approach the resonant wavelength where the shift of the resonant wavelength will induce a large fluctuation of output voltage. The measured maximum voltage variation is down to 0.011 V for 30 min, and the calculated change of wavelength is less than 20 pm. The corresponding instability in relative humidity measurement is 0.873%RH, indicating a good stability of the sensor.

Finally, we investigated the hysteresis effect, reversibility, and repeatability of the developed sensor. In order to obtain a stable sensor, it was annealed at 85°C with the relative

humidity keeping at 90%RH for 100 h [20]. The resonant wavelength has a slight blue shift of 1.354 nm after annealing. In Fig. 7(a), a sensitivity of 22.8 ± 1.92 pm/%RH and 22.53 ± 1.97 pm/%RH were measured for increasing and decreasing, respectively. A maximum hysteresis error of 1.17% occurs when RH was adjusted from high to low values. The weak non-coincidence caused by hysteresis is acceptable with error tolerance. Figure 7(b) shows its linear dependence on relative humidity at three different temperatures. The sensor exhibits a sensitivity of 22.8 ± 1.92 pm/%RH, 22.42 ± 1.99 pm/%RH, and 22.44 ± 2.07 pm/%RH for increasing in RH at 25°C, 35°C, and 40°C, respectively. The corresponding sensitivity for decreasing in RH is 22.53 ± 1.95 pm/%RH, 22.38 ± 2.03 pm/%RH, and 22.2 ± 2.15 pm/%RH. The sensitivity at 50°C is decreased into 18.3 ± 2.07 pm/%RH. Thus, the developed sensor keeps consistent sensitivity from 25°C to 40°C. At this temperature range, the shift in resonant wavelength caused by temperature is 10.3 pm/K, which is much less than the value of 78 pm/K of silicon nanobeam cavities reported in the literature [21]. This is attributed to the PMMA of negative thermo-optic coefficient (TOC) having a compensation of positive temperature dependence of the fabricated silicon nanobeam cavity. The consistent sensitivities and weak shift in resonant wavelength demonstrate that this developed sensor is temperature insensitive from 25°C to 40°C. A lower temperature dependence is expected to achieve by changing the thickness of the PMMA cladding. The humidity sensor can be widely applied in a variety of areas, such as weather forecasting, foodstuff preservation in agriculture, and industrial process control in semiconductor fabrication. Finally, in order to investigate the reversibility and repeatability, it was placed in the closed chamber with RH changing from 40%RH to 80%RH for several cycles over a period of 4.2 h. The resonant wavelength shift can reach the consistent shift for five cycles, as shown in Fig. 7(c). It demonstrates that the sensor possesses a good reversibility and repeatability from 40%RH to 80%RH. A weak fluctuation in resonant wavelength shift is caused by errors in controlled humidity (80 ± 0.5 %RH, 40 ± 0.5 %RH). The average shift is 0.918 nm, and the corresponding sensitivity is 22.9 pm/%RH, which agrees with value of 22.8 ± 1.9 pm/%RH above.

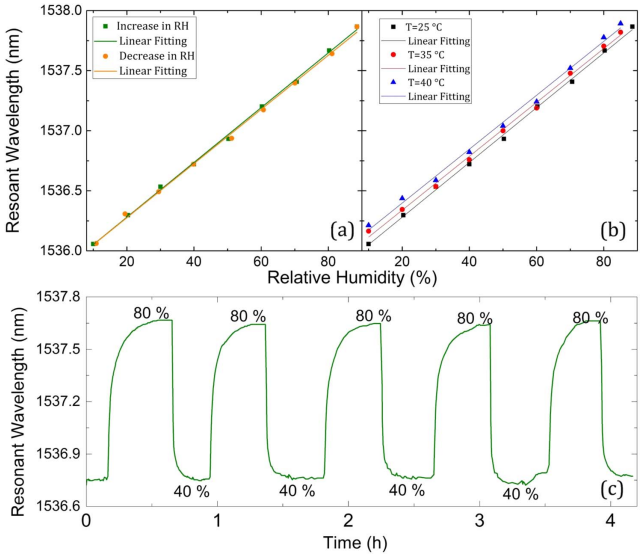

Fig. 7. (a) Dependence of resonant wavelength on RH. (b) Relationship between resonant wavelength and RH at different temperatures. (c) Recorded resonant wavelength for five cycles from 40%RH to 80%RH.

In conclusion, a humidity sensor based on a chip-scale silicon nanobeam cavity with PMMA cladding has been demonstrated. Among various thickness of PMMA cladding, the sensor with 500-nm-thick possesses the maximum sensitivity. The sensor is expected to achieve a higher sensitivity and temperature range by substituting some new materials for PMMA as its upper cladding. It is also suitable for developing other types of sensors by choosing corresponding sensing material as cladding. As far as we know, the combination of humidity detecting with chip-scale silicon nanobeam cavities is achieved for the first time, which greatly promotes the development of integrated sensing and optical systems in the future.

Funding. National Key RD Program of China (2017YFB1002501); 863 Program (2013AA014402); National Natural Science Foundation of China (61728402); Research Program of Shanghai Science and Technology Committee (17JC1402800).

Acknowledgment. The authors are also grateful to the Center for Advanced Electronic Materials and Devices (AEMD) of Shanghai Jiao Tong University.

REFERENCES

1. J. M. Lopez-Higuera, L. Rodriguez Cobo, A. Q. Incera, and A. Cobo, J. Lightwave Technol. **29**, 587 (2011).
2. Q. Kuang, C. Lao, Z. L. Wang, Z. Xie, and L. Zheng, J. Am. Chem. Soc. **129**, 6070 (2007).
3. W. Zhang and D. J. Webb, Opt. Lett. **39**, 3026 (2014).
4. H. Guan, K. Xia, C. Chen, Y. Luo, J. Tang, H. Lu, J. Yu, J. Zhang, Y. Zhong, and Z. Chen, Opt. Mater. Express **7**, 1686 (2017).
5. T. Venugopalan, T. Sun, and K. T. V. Grattan, Sens. Actuators A, Phys. **148**, 57 (2008).
6. T. Li, X. Dong, C. C. Chan, K. Ni, S. Zhang, and P. P. Shum, IEEE Sens. J. **13**, 2214 (2013).
7. Y. Luo, C. Chen, K. Xia, S. Peng, H. Guan, J. Tang, H. Lu, J. Yu, J. Zhang, Y. Xiao, and Z. Chen, Opt. Express **24**, 8956 (2016).
8. Y. Wang, C. Shen, W. Lou, F. Shentu, C. Zhong, X. Dong, and L. Tong, Appl. Phys. Lett. **109**, 031107 (2016).
9. C. Li, X. Yu, W. Zhou, Y. Cui, J. Liu, and S. Fan, Opt. Lett. **43**, 4719 (2018).
10. Y. Peng, Y. Zhao, M.-Q. Chen, and F. Xia, Small **14**, 1800524 (2018).
11. L. Alwis, T. Sun, and K. T. V. Grattan, Sens. Actuators B Chem. **178**, 694 (2013).
12. D. A. Avila Padilla, C. O. T. Moreno, and C. M. B. Cordeiro, J. Phys. Conf. Ser. **792**, 12050 (2017).
13. F. Liang, Y. Guo, S. Hou, and Q. Quan, Sci. Adv. **3**, e1602991 (2017).
14. Y. Chen, W. S. Fegadolli, W. M. Jones, A. Scherer, and M. Li, ACS Nano **8**, 522 (2013).
15. L. Stern, A. Naiman, G. Keinan, N. Mazurski, M. Grajower, and U. Levy, Optica **4**, 1 (2017).
16. H. Xu, M. Hafezi, J. Fan, J. M. Taylor, G. F. Strouse, and Z. Ahmed, Opt. Express **22**, 3098 (2014).
17. Y. Zhang, S. Han, S. Zhang, P. Liu, and Y. Shi, IEEE Photon. J. **7**, 6802906 (2015).
18. B. Y. Y. Zhao, Sens. Actuators B Chem. **271**, 256 (2018).
19. J. S. Santos, I. M. Raimundo, C. M. B. Cordeiro, C. R. Biazoli, C. A. J. Gouveia, and P. A. S. Jorge, Sens. Actuators B Chem. **196**, 99 (2014).
20. G. Woyessa, K. Nielsen, A. Stefani, C. Markos, and O. Bang, Opt. Express **24**, 1206 (2016).
21. N. Klimov, T. Purdy, and Z. Ahmed, Sens. Actuators A, Phys. **269**, 308 (2018).